



**HAL**  
open science

# The Hidden Spatial Dimension of Alpha: 10-Hz Perceptual Echoes Propagate as Periodic Traveling Waves in the Human Brain

Diego Lozano-Soldevilla, Rufin Vanrullen

► **To cite this version:**

Diego Lozano-Soldevilla, Rufin Vanrullen. The Hidden Spatial Dimension of Alpha: 10-Hz Perceptual Echoes Propagate as Periodic Traveling Waves in the Human Brain. *Cell Reports*, 2019, 26 (2), pp.374-380.e4. 10.1016/j.celrep.2018.12.058 . hal-03093455

**HAL Id: hal-03093455**

**<https://hal.science/hal-03093455>**

Submitted on 3 Jan 2021

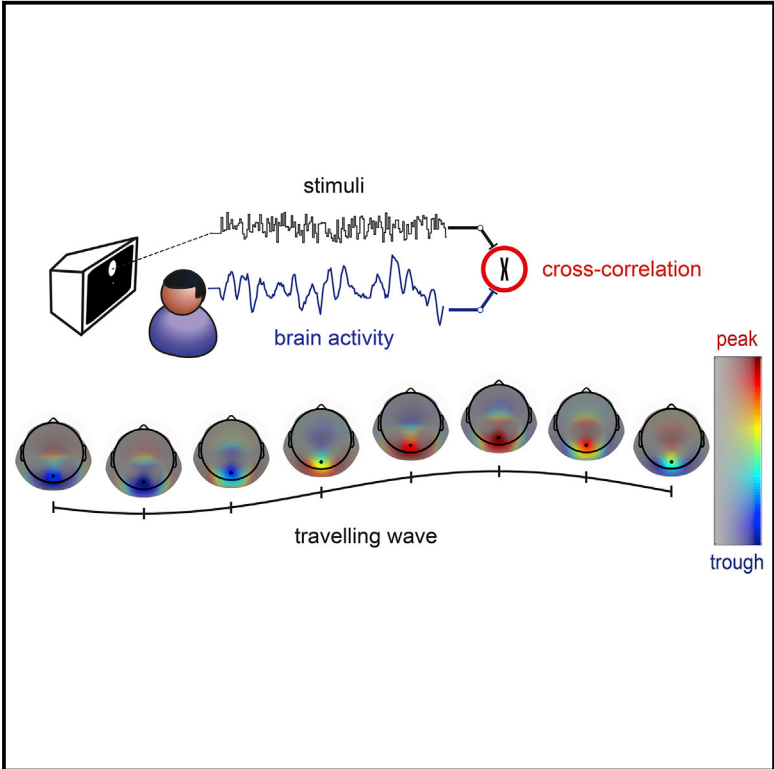
**HAL** is a multi-disciplinary open access archive for the deposit and dissemination of scientific research documents, whether they are published or not. The documents may come from teaching and research institutions in France or abroad, or from public or private research centers.

L'archive ouverte pluridisciplinaire **HAL**, est destinée au dépôt et à la diffusion de documents scientifiques de niveau recherche, publiés ou non, émanant des établissements d'enseignement et de recherche français ou étrangers, des laboratoires publics ou privés.

# Cell Reports

## The Hidden Spatial Dimension of Alpha: 10-Hz Perceptual Echoes Propagate as Periodic Traveling Waves in the Human Brain

### Graphical Abstract



### Authors

Diego Lozano-Soldevilla, Rufin VanRullen

### Correspondence

rufin.vanrullen@cnrs.fr

### In Brief

Alpha oscillations are key players in visual processing. Lozano-Soldevilla and VanRullen demonstrate that the ~10-Hz component of perceptual echoes behaves as a traveling wave, coding stimuli presented in different visual hemifields with consistent phase differences, like the beam of a radar scanning the field.

### Highlights

- Perceptual echoes behave as traveling waves
- Perceptual echoes show systematic phase differences across scalp contacts
- Perceptual echoes show systematic phase differences across visual hemifields
- Perceptual echoes scan the visual field rhythmically



# The Hidden Spatial Dimension of Alpha: 10-Hz Perceptual Echoes Propagate as Periodic Traveling Waves in the Human Brain

Diego Lozano-Soldevilla<sup>1,2</sup> and Rufin VanRullen<sup>1,2,3,\*</sup>

<sup>1</sup>CNRS, UMR5549, Centre de Recherche Cerveau et Cognition, Faculté de Médecine de Purpan, Toulouse, France

<sup>2</sup>Université Paul Sabatier, Toulouse, France

<sup>3</sup>Lead Contact

\*Correspondence: [rufin.vanrullen@cnrs.fr](mailto:rufin.vanrullen@cnrs.fr)

<https://doi.org/10.1016/j.celrep.2018.12.058>

## SUMMARY

EEG reverse-correlation techniques have revealed that visual information processing entails a  $\sim 10$ -Hz (alpha) occipital response that reverberates sensory inputs up to 1 s. However, the spatial distribution of these perceptual echoes remains unknown: are they synchronized across the brain, or do they propagate like a traveling wave? Here, in two experiments with varying stimulus locations, we demonstrate the systematic phase propagation of perceptual echoes. A single stimulation in the upper visual field produced an “echo traveling wave” propagating from posterior to frontal sensors. The simultaneous presentation of two independent stimuli in separate visual hemifields produced two superimposed traveling waves propagating in opposite directions. Strikingly, in each sensor, the phase of the two echoes differed, with a phase advance for the contralateral stimulus. Thus, alpha traveling waves sweep across the human brain, encoding stimulus position in the phase domain, in line with the 70-year-old “cortical scanning” hypothesis (Pitts and McCulloch, 1947).

## INTRODUCTION

The alpha rhythm (8–12 Hz) is the most prominent spectral fingerprint in the human brain, and its functional role is an active area of research. After stimulus onset, alpha oscillations show a well-characterized amplitude reduction (i.e., desynchronization) whose magnitude can be interpreted as a measure of task efficiency (Pfurtscheller and Lopes da Silva, 1999). Conversely, transient visual stimulation also produces brief positive and negative voltage deflections (event-related potentials [ERPs]) that last 100–500 ms and that correlate with perception (Hillyard et al., 1998). Importantly, these transient ERPs vanish very quickly unless external stimulation is provided. A recent study from our laboratory revealed a new time-locked  $\sim 10$ -Hz oscillatory component that could last more than 1 s and that was thus dubbed “perceptual echo” (VanRullen and Macdonald, 2012). Stimulating participants with white-noise luminance sequences

(i.e., equal power at all temporal frequencies) produced frequency-specific  $\sim 10$ -Hz reverberations in posterior sensors (Ilhan and VanRullen, 2012; VanRullen and Macdonald, 2012). These echoes could be revealed by averaging the single-trial cross-correlations between the electroencephalographic (EEG) recordings and the luminance values of the random sequences (Lalor et al., 2006; VanRullen and Macdonald, 2012), yielding an estimate of the impulse response function (IRF) (Marmarelis and Marmarelis, 1978). In other words, the perceptual echoes reflect changes in EEG brain activity proportional to luminance changes for different lags (i.e., cross-correlation). The perceptual echoes are a true response to the information contained in the visual stimulus sequence: shuffling the pairing between luminance sequences and EEG time series practically abolishes the  $\sim 10$ -Hz oscillation (VanRullen and Macdonald, 2012). This is in clear contrast to traditional ERPs, which do not quantify (nor correlate) single-trial EEG amplitude fluctuations as a function of the strength of a stimulus feature. The presence of long-lasting reverberations in this IRF (or perceptual echoes) implies that alpha oscillations are the optimal resonant frequency of the visual system, and that the brain can carry information about the stimuli content for more than 1 s (Ilhan and VanRullen, 2012; VanRullen and Macdonald, 2012; Brüers and VanRullen, 2017). In sum, perceptual echoes are a direct correlate (quantified by a correlation metric) of stimulus information processing.

It is not known, however, whether  $\sim 10$ -Hz perceptual echoes from a particular visual field location reverberate across the cortex simultaneously or asynchronously. Moreover, does stimulation over multiple visual coordinates evoke multiple echoes, and are these oscillations uniform or do they show consistent phase differences? In order to investigate the spatial dimension of perceptual echoes, we re-analyzed two datasets (VanRullen and Macdonald, 2012; Brüers and VanRullen, 2017) to probe the existence of systematic phase variations across visual and/or cortical space.

## RESULTS

### Perceptual Echoes Travel Rhythmically through the Scalp

Observers ( $n = 28$ ) were stimulated with white-noise luminance sequences of 6.25-s duration at a single, fixed location, while EEG recordings were simultaneously acquired. Luminance



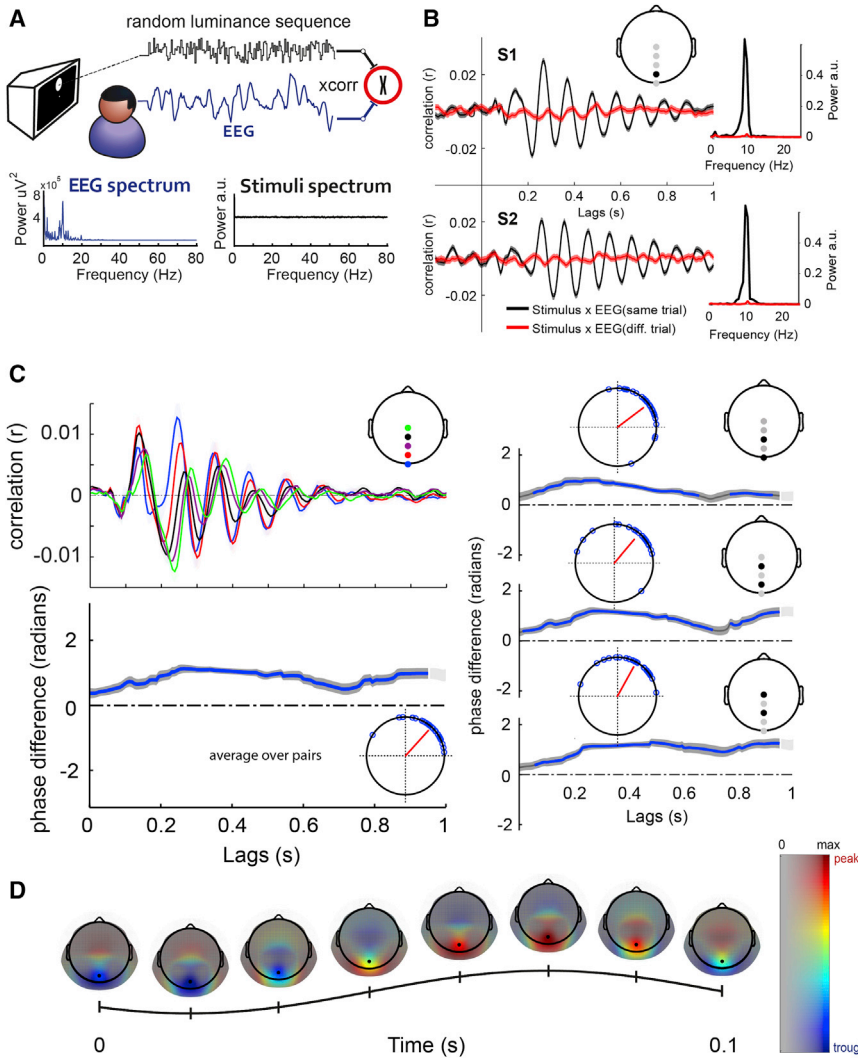


**Figure 1. Visual Input from a Single Location Produces a Bilateral, Occipital-to-Parietal Oscillatory Traveling Wave**

(A) In experiment 1, random white-noise luminance sequences (black trace) were presented to the participants while EEG (blue trace) was simultaneously acquired. Perceptual echoes (or IRF) are the averaged cross-correlations between the luminance sequence and the simultaneously acquired EEG time series. Bottom: illustration of the power spectrum of a single-trial EEG and of a single-trial luminance sequence.

(B) Perceptual echoes of two participants (left) and their corresponding power spectrum representations (right). Echoes were computed by averaging the cross-correlations between stimuli and EEG trials (black) or shuffling the trial order between them (red). Shaded areas represent SEM across trials.

(C) Left top: grand-mean ( $n = 28$ ) echo functions from sensors Oz (blue), POz (red), Pz (purple), CPz (black), and Cz (green; shaded areas represent SEM across participants). Perceptual echoes in parieto-occipital sensors showed a gradual and constant phase change from posterior to anterior sensors. Left bottom: grand-mean ( $n = 28$ ) time-resolved analytic phase differences of the alpha band of the two perceptual echoes averaged across sensor pairs. Right: time-resolved analytic phase differences for each sensor pair of interest (see right insert for each subplot). Shaded areas represent SEM across participants, and areas with high contrast (dark gray) represent significant phase relation consistent across participants (significant PLV; see STAR Methods). The blue line represents time points where the phase difference is significantly different from zero (one-sample mean angle test;  $p < 0.05$ ). The inserted Argand plots show the phase difference of the channel pair and its corresponding vector strength pointing toward the mean angle. Each dot represents the phase difference for a single participant.

(D) Single-cycle wave template of the alpha component of perceptual echoes. The template

was computed by averaging over the PLV significant time period the analytic pairwise phase differences between a reference electrode (POz black) and the rest of the EEG (see STAR Methods and Figure S1). The time axis represents a single cycle of a 10-Hz wave and the associated topoplots are snapshots within this single time period, arbitrarily chosen between 0 and 0.1 s. The x axis of the two-dimensional (2D) color bar represents the amplitude of the peak of the echo in levels of gray. Sensors with small echo amplitude have high gray values (less transparent) and sensors with large echo amplitude have low gray values (more transparent). The y axis of the 2D color bar represents the instantaneous voltage of the sine wave (jet color map). For visualization purposes, topographies were masked with gray transparency values proportional to the peak amplitude of the perceptual echo, raised to the power of 3.

changes were displayed within a peripheral disc presented above the fovea, and participants had to covertly attend to it while maintaining fixation (Figure 1A). Cross-correlating the flickering sequences and the simultaneously acquired EEG recordings (Lalor et al., 2006; VanRullen and Macdonald, 2012), robust correlation values oscillating around the alpha rhythm were found in the IRF (Figure 1B). The magnitude of the grand mean correlations ( $r \sim 0.01$ ; Figure 1C) was smaller than in individual averages ( $r \sim 0.02$ ; Figure 1B). This was mainly due to differences in the onset and frequency of the IRF across participants (Figure 1B; the echoes in participants S1 and S2 show strong phase misalignment after lag of  $\sim 0.5$  s); the magnitude of the grand mean is necessarily lower relative to the contribution of individual

estimates. A similar decrease was found by İlhan and VanRullen (2012). To estimate the spatial propagation of perceptual echoes through the scalp, we computed the phase difference between non-contiguous midline parieto-occipital sensor pairs: Oz-Pz, POz-CPz, and Pz-Cz. The resulting phase-locking value (PLV) for this phase difference was averaged over all pairs and participants (see STAR Methods). We found that participants showed a consistent phase relationship between the echoes evoked at different parieto-occipital scalp locations over the lag period from 0 to 0.95 s (Figure 1C, dark gray; significant PLV,  $p < 0.01$ , comparison with surrogate distribution of PLV under the null hypothesis, false-discovery rate [FDR] corrected). Note that these significant PLV values do not inform about the magnitude of the

phase difference (only about the consistency of phase relations). For example, the activity of two EEG sensors could be always synchronous (i.e., zero phase lag) or there might be a systematic lag or lead between responses (i.e., periodic traveling wave). To disentangle between the two possibilities, we examined the direction of the phase relationship. For this, we computed analytic phase differences within the alpha range (8–12 Hz) between the sensor pairs of interest (Figure 1C, right inserts). The three pairwise comparisons and their average showed a significant and consistently positive pattern of phase differences (Oz-Pz, one-sample mean angle test,  $p < 0.05$ ; mean angle = 0.6461; Rayleigh  $z = 19.72$ ;  $p = 1.8 \times 10^{-11}$ ; POz-CPz, one-sample mean angle test,  $p < 0.05$ ; mean angle = 0.8704; Rayleigh  $z = 18.03$ ;  $p = 3 \times 10^{-10}$ ; Pz-Cz, one-sample mean angle test,  $p < 0.05$ ; mean angle = 1.07; Rayleigh  $z = 20.60$ ;  $p = 3.8 \times 10^{-12}$ ; average over pairs, one-sample mean angle test,  $p < 0.05$ ; mean angle = 0.8362; Rayleigh  $z = 21.91$ ;  $p = 3.1 \times 10^{-13}$ ; see blue lines and left circular histogram inserts in Figure 1C). These results indicate that perceptual echoes systematically propagated from posterior (Oz) to central (Cz) channels with an average delay of  $\sim 34$  ms (corresponding to an Oz-Cz phase difference of  $\sim 2\pi/2.8$ ).

We observed consistent phase differences between sensors (i.e., non-zero phase lag), forming a spatio-temporal pattern of narrow-band oscillatory activity that propagated gradually through space (i.e., across the scalp) during several cycles, in other words, a periodic traveling wave (Hughes, 1995; Prechtl et al., 2000; Ermentrout and Kleinfeld, 2001). Specifically, posterior electrodes (Oz; blue trace, Figure 1C) lead the periodic wave propagation of activity relative to more anterior electrodes (Cz; green trace, Figure 1C). To characterize the spatial propagation of perceptual echoes, we constructed a wave template using the grand-mean perceptual echoes (Figure 1D; see STAR Methods and Figure S1). We band-pass filtered the alpha component of the perceptual echoes, and we computed all pairwise phase differences between a reference sensor showing the strongest echo (i.e., POz) and the rest of the scalp, averaged over the significant time lags found in Figure 1C (average over pairs). Figure 1D shows the wave template evolution over a single alpha cycle ( $0-2\pi$ ; 100-ms duration). Perceptual echoes behaved as periodic traveling waves, whose propagation initiated over occipital sensors and flowed toward frontal sensors during several oscillatory cycles (Video S1). This means that information processing for these stimuli, indexed by cross-correlation values in the IRF, was tightly linked to an alpha wave that traveled rhythmically in a posterior-to-anterior direction.

### Perceptual Echoes Scan the Visual Field Sequentially Every $\sim 100$ ms

The above observations suggest that perceptual echoes do not emerge synchronously over the entire scalp. To go one step further, we analyzed the data of a second experimental condition, in which two independent white-noise luminance sequences were simultaneously presented on respective discs to the left and right of the fixation point (Figure 2A). Can a single cortical region (or scalp channel) simultaneously respond with an echo to each visual location? If yes, would the two echoes unfold synchronously, or show consistent phase differences? Experiment 2 ( $n = 10$ ) allowed us to test two spatial dimensions

of perceptual echoes: visual (i.e., comparing screen coordinates) and cortical (i.e., comparing scalp coordinates).

To test how perceptual echoes differed across distinct visual coordinates (i.e., stimuli located in the left and right visual hemifields), we computed cross-correlation analysis between the EEG and each luminance sequence separately (Figure 2A). On each occipito-parietal EEG sensor, we found two independent echo responses evoked by the respective stimuli sequences (Figure 2B). In order to estimate the time lags for which perceptual echoes in response to the two simultaneous flickering sequences showed a systematic phase relation, we computed the PLV across participants of the phase difference between the two echoes. Briefly, for each participant and EEG sensor, we bandpass filtered the alpha component of perceptual echoes in response to the two flicker sequences. We obtained the analytic phase of the filtered alpha band using the Hilbert transform. Then, for each participant, we computed the magnitude of the phase difference between the left and right perceptual echoes; the PLV for this phase difference was finally computed over participants (and averaged over all sensors; see STAR Methods). We found that participants showed a consistent phase relationship between the echoes evoked by the discs located in each visual hemifield over the lag period from 0.15 to 0.6 s ( $p < 0.01$ , comparison with surrogate distribution of PLV, FDR corrected). To investigate potential phase lags and associated wave patterns, we focused on lateralized sensors of interest, and we computed the alpha-band analytic phase differences between left versus right perceptual echoes (Figure 2B). While the left sensor revealed significant negative non-uniform phase differences (one-sample mean angle test,  $p < 0.05$ ; mean angle =  $-0.8034$ ; Rayleigh  $z = 6.388$ ;  $p = 6.2 \times 10^{-4}$ ; Figure 2B, bottom left, blue line), the right one showed complementary positive non-uniform phase differences (one-sample mean angle test,  $p < 0.05$ ; mean angle = 0.6529; Rayleigh  $z = 6.581$ ;  $p = 4.7 \times 10^{-4}$ ; Figure 2B, bottom right, blue line). These results indicate that perceptual echoes measured in contralateral sensors were leading (i.e., statistically significant phase advance) relative to their ipsilateral homologs.

### Two Stimuli Can Generate Two Simultaneous Periodic Traveling Waves

As in experiment 1, we mapped the analytic phase of the alpha component of perceptual echoes in response to each given stimulus, separately for left and right sensors. For the left stimulus, we found statistically significant negative phase differences, meaning that right parietal sensors showed a phase advance relative to the left sensors (Figure 3A). Complementary results (i.e., positive phase difference) were found for the right stimulus. In both analyses, the mean phase difference was around  $\pi/2.4$  corresponding approximately to a  $\sim 21$ -ms delay (left stimuli: left minus right sensor, mean angle =  $-0.9982$  radians; Rayleigh  $z = 5.6382$ ;  $p = 0.0018$ ; Figure 3A, bottom left, blue line; right stimuli: mean angle = 1.3519 radians; Rayleigh  $z = 6.225$ ;  $p = 7.9 \times 10^{-4}$ ; Figure 3A, bottom right, blue line). As done previously, we characterized the spatiotemporal propagation of perceptual echoes by computing a wave template. For each perceptual echo in response to each stimuli sequence, we

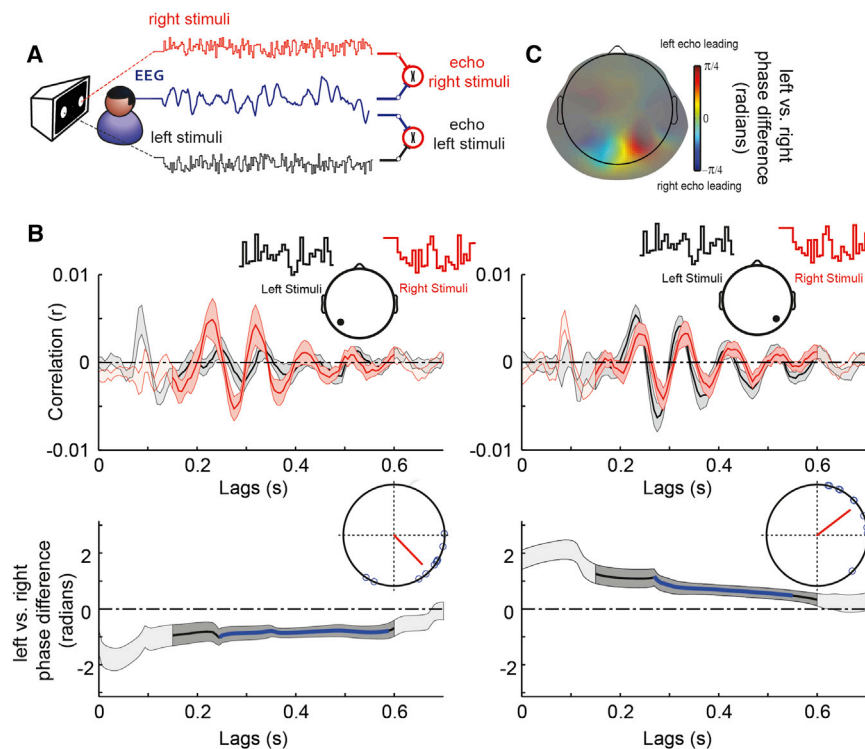


**Figure 2. Spatial Propagation of Perceptual Echoes in the Visual Domain (Phase Differences between Screen Locations)**

(A) In experiment 2, two independent random white-noise luminance sequences were presented to the participants while EEG was simultaneously acquired. Two sets of single-trial cross-correlations between each stimuli sequence and the EEG were carried out, to compute the average echo in response to right stimuli (in red throughout the figure) and the average echo in response to left stimuli (black).

(B) Top: grand-mean ( $n = 10$ ) perceptual echoes measured at a single sensor of interest (topographic inserts) in response to the two stimuli sequences. Shaded areas represent SEM across participants and areas with high contrast represent significant phase relation consistent across participants (PLV; see STAR Methods). Bottom: time-resolved analytic phase differences (left minus right echoes) of the alpha-band component of the two perceptual echoes measured in one sensor of interest. Shaded areas represent SEM across participants and areas with high contrast represent significant phase relation consistent across participants (PLV). The blue line represents time points where the phase difference is significantly different from zero (one-sample mean angle test;  $p < 0.05$ ). Here, we see that the contralateral stimulus location had a systematic phase advance relative to the ipsilateral one. The inserted Argand

plots show the phase difference of the left versus right stimuli and its corresponding vector strength pointing toward the mean angle.

(C) Grand-mean topographic representation of phase differences (left minus right perceptual echoes) averaged over the time period showing a significant phase relation consistent across participants (PLV). Color code represents phase differences in radians. For visualization purposes, topographies were masked with gray transparency values proportional to the peak amplitude of the perceptual echo, raised to the power of 3.

computed all pairwise phase differences between a reference sensor of interest (POz) and the rest of the EEG. We found that each template wave propagated mainly in the contralateral to ipsilateral direction (Figure 3B). Strikingly, these two periodic traveling waves happened simultaneously and were therefore superimposed on the scalp (Video S2); they were disentangled here by reverse-correlation techniques.

## DISCUSSION

Here, we demonstrate the hidden dimension of perceptual echoes: its spatial propagation. We show that perceptual echoes are periodic traveling waves that not only propagate across the cortex during several cycles but they also display phase differences between different spatial coordinates of the visual field in most of our 38 participants, like a radar beam scanning the field. In experiment 1, the stimulus located above the fovea generated a single periodic traveling wave, to which the two hemispheres contributed with coherent activity, propagating from posterior to frontal sensors during multiple alpha cycles. In experiment 2, we showed that two independent random flickering sequences located in the two visual hemifields generated two superimposed periodic traveling patterns, whose phase propagation traveled following the contralateral to ipsilateral direction. As a result, the two perceptual echoes recorded at a given scalp location showed a sequential activation: periodic

waves in response to contralateral stimulation were phase-advanced relative to ipsilateral stimulation.

We can be reasonably confident that the periodic traveling waves recorded across the scalp surface in the two experiments actually reflect spatial propagation of activity within and/or between specific brain regions. Because electrical conduction delays are negligible, a single static source would necessarily produce synchronized oscillations across the entire scalp, with opposite polarities on the two sides of the equivalent current dipole, but no smooth phase transitions (this is typically called a “standing wave”). Thus, in order to produce smooth phase changes, there must be at least two or more underlying oscillatory sources with a consistent phase difference between them; this is actually the minimal definition for a “periodic traveling wave” (Hughes, 1995; Ermentrout and Kleinfeld, 2001). Nonetheless, we acknowledge that whether these multiple oscillatory sources span a large cortical extent or a very small one (making the effect mathematically similar to a rotating dipole) remains an open question; our equivalent current dipole (ECD) modeling efforts (reported in Figures S2–S4) suggest that both local and global hypotheses (as well as intermediate ones) are viable. With this in mind, the present results demonstrate that perceptual echoes behave like periodic traveling waves. To our knowledge, this is the first demonstration of two concurrent and overlapping stimulus-induced periodic traveling waves in humans.

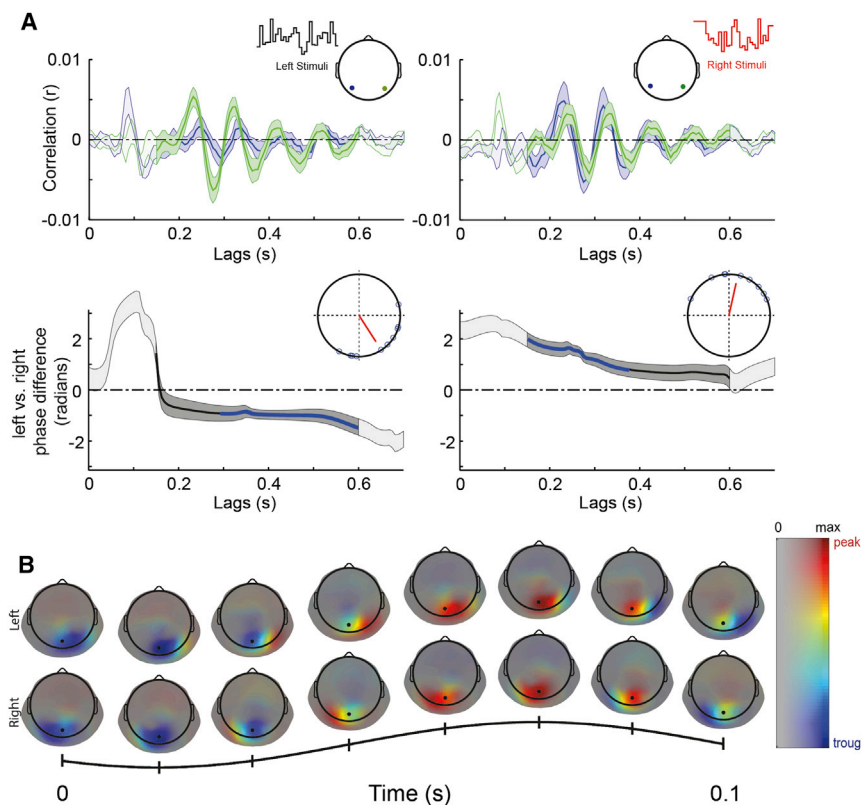


**Figure 3. Spatial Propagation of Perceptual Echoes in the Scalp Domain (Phase Differences between Scalp Locations)**

(A) Top: grand-mean ( $n = 10$ ) perceptual echoes measured at two sensors of interest (topographic inserts) in response to left stimuli sequences (left-hand side) or right stimuli sequences (right-hand side). Shaded areas represent SEM across participants, and areas with high contrast represent significant phase relation consistent across participants (PLV; see STAR Methods). Bottom: time-resolved analytic phase differences (left minus right electrodes) of the alpha band of the perceptual echoes. Shaded areas represent SEM across participants and areas with high contrast represent significant phase relation consistent across participants (PLV). The blue line represents time points where the phase difference is significantly different from zero (one-sample mean angle test;  $p < 0.05$ ). Here, we see that the contralateral scalp location had a systematic phase advance relative to the ipsilateral one. The inserted Argand plots show the phase difference of the left versus right stimuli and its corresponding vector strength pointing toward the mean angle.

(B) Single-cycle wave template of the alpha component of perceptual echoes in response to left (top) and right (bottom) luminance sequences. The template was computed by averaging over the time period 0.15–0.6 s the analytic pairwise phase differences between a reference electrode (POz black) and the rest of the EEG (see STAR Methods). Color code and mask with same conventions as in Figure 1D.

While previous resting-state human EEG studies reported anterior-to-posterior propagation dynamics (Nunez et al., 2001; Nolte et al., 2008), visual stimulation experiments produced ERPs containing an alpha-frequency component that propagated from posterior to anterior sensors (Shevelev et al., 2000; Klimesch et al., 2007). The present results constitute a significant step forward for several reasons. First, contrary to ERPs that measure voltage variations and can only be indirectly related to stimulus properties (Fellinger et al., 2012; Alexander et al., 2013), the perceptual echoes (or so-called IRFs) directly reflect sensory information processing, indexed by cross-correlation coefficients between EEG and luminance sequences. Second, the resulting correlations (i.e., perceptual echoes) obeyed simple retinotopic rules (i.e., contralateral-to-ipsilateral propagation), which implies that they follow the structure and functional organization of basic cortical pathways. Third, we were able to simultaneously induce two overlapping periodic traveling waves propagating in distinct directions (Video S2). Finally, another aspect of the present traveling waves worth insisting on is their periodic nature. Classic studies in monkeys have found traveling waves mainly during resting-state conditions (Ermentrout and Kleinfeld, 2001), but more recent studies have shown that sensory stimulation using periodic stimuli also produces traveling waves, whereby for each new stimulus cycle a single wavefront propagates through cortical space (Sato et al., 2012; Muller et al., 2014). However, these traveling waves are different from the periodic traveling waves found here in which perceptual

echoes evoked by random (aperiodic) stimulation maintain their periodicity during four or more consecutive cycles.

What could be the neurophysiological mechanisms underlying the consistent phase differences we observed at the scalp level? A straightforward explanation could be that perceptual echoes propagate across a large portion of cortical space. More concretely, multiple neuronal patches of occipito-parietal cortex could be activated in a chain reaction (i.e., phase delays between neuronal pools); in this way, the scalp phase differences would directly mirror underlying cortical phase differences. Our ECD analysis on the positive rectified topographical template suggests that this is indeed one valid possibility (Figures 1D, 3B, and S2–S4). However, due to the well-known limitations of noninvasive source reconstruction (Lütkenhöner, 2003), there are alternative explanations to consider. Mathematically, a periodic traveling wave measured at the scalp can also be reduced to a static dipole(s) whose orientation rotates as a function of time, producing an “apparent” propagation that can be measured with EEG by volume conduction. A hypothetical pool of neurons would synchronize its firing activity around the alpha band, and its dipole moment would rotate in space (e.g., from contralateral to ipsilateral direction along the parieto-occipital cortex; Figures 1D and S2). This would produce consistent phase differences in the sensor domain, because the dipole would project its peak electrical voltage at various points in the channel space as a function of time. However, this mathematically valid construct has no direct physiological

equivalent: taking the rotating dipole hypothesis literally would imply that the axons of the hypothetical pool of neurons would physically rotate around the soma every 100 ms! A more plausible physiological interpretation would consist in a spatially restricted wave activation pattern that propagates locally, through sulci and gyri of varying orientation, resulting in a global periodic traveling pattern at the scalp level. This is known as the intra-cortical hypothesis, which assumes that phase differences at the scalp level reflect the geometric curvature of the wave propagation (Hindriks et al., 2014). In this case, however, there would still be a periodic wave of activity traveling over cortical space, only with a much more restricted spatial extent. Our ECD modeling on the unrectified wave template is also compatible with this interpretation. A third possibility, the 2-dipole phase-lagged traveling wave (in which only 2 dipoles oscillate with a fixed phase difference) can be thought of as an intermediate point in a continuum between the global and local situations. Future studies using magnetoencephalographic and preferably electrocorticographic (ECoG) recordings would be instrumental in determining the origin and propagation pattern of perceptual echoes. Two very recent human ECoG studies show that alpha oscillations were present over multiple brain areas and they propagated through extended parts of the cortex in a posterior-to-anterior direction (Zhang et al., 2018) but also in the opposite direction (Halgren et al., 2017). Another recent ECoG study found that sleep spindle activity forms spontaneous circular traveling waves that repeat themselves multiple times over several hours and that might help to store and integrate memories in humans (Muller et al., 2016).

Overall, it is unavoidable that the periodic traveling wave observed at the scalp originates from a traveling wave in the brain, although we cannot precisely pinpoint its spatial extent: local propagation versus large-scale propagation over multiple brain regions. Depending on its exact spatial extent, the spatial propagation of the traveling wave may reflect several (non-exclusive) underlying processes: (1) a (periodic) feed-forward pass of activity through the hierarchy of visual areas, from V1 to posterior parietal cortex; (2) horizontal connections linking various portions of retinotopic space, potentially through iso-centric functional connections (Arcaro et al., 2015); and/or (3) inputs from subcortical structures of the thalamus, such as the pulvinar (da Silva et al., 1973), a neural communication “hub” that has been demonstrated to participate in the oscillatory coordination of activity between occipital and parietal areas at alpha frequency (Saalman et al., 2012). Future studies would be needed to disentangle these underlying neural mechanisms.

What could be the functional advantage of a traveling perceptual echo spanning several cycles (Muller et al., 2018)? Two previous studies have shown that perceptual echoes modulate behavior. The original study showed that, in a version of the task in which the participants were instructed to move the joystick as a function of the degree of perceived flicker intensity, the energy of the stimuli between 8 and 15 Hz was the perceptually relevant one (Figure 4A of VanRullen and Macdonald, 2012). This suggests that perceptual echoes are the impulse “perceptual” filter that extracts the alpha energy of the external stimulation, yielding a subjective impression of a regular flicker, even

when the stimuli are random. More recently, Brüers and VanRullen (2017) showed a modulation of behavioral performance as a function of the phase of perceptual echoes. How behavioral performance varies as a function of the propagation of the traveling wave remains an open question for future studies. We showed consistent phase differences in the scalp domain (i.e., when comparing different sensors) and in the visual domain (i.e., when comparing the echoes produced by two simultaneous flickering stimuli located in separate hemifields). This could be explained as a wave (or a number of simultaneous waves) sequentially scanning different parts of the cortex as a function of visual stimulation coordinates. To make an analogy, perceptual echoes would behave similarly as the beam of a radar scanning the field. Every cycle of the beam of the radar (perceptual echo) would sweep the visual field rhythmically. As a result, different parts of the visual field are sampled at different times, in a specific order (Video S3). Similarly, different regions of the cortical hierarchy are sampled at different times and in a specific order (Videos S1 and S2). We speculate that this is in line with what Pitts and McCulloch (1947) conjectured 70 years ago in the “cortical scanning” hypothesis: “this alpha rhythm performs a temporal ‘scanning’ of the cortex which thereby gains, at the cost of time, the equivalent of another spatial dimension in its neural manifold.” Here, we presented evidence that supports the existence of such an additional spatial dimension in sensory cortex, encoded in the phase of the alpha oscillatory cycle of perceptual echoes.

## STAR★METHODS

Detailed methods are provided in the online version of this paper and include the following:

- KEY RESOURCES TABLE
- CONTACT FOR REAGENT AND RESOURCE SHARING
- EXPERIMENTAL MODEL AND SUBJECT DETAILS
- METHOD DETAILS
  - Design, Procedure and Materials
- QUANTIFICATION AND STATISTICAL ANALYSIS
- DATA AND SOFTWARE AVAILABILITY

## SUPPLEMENTAL INFORMATION

Supplemental Information includes four figures and three videos and can be found with this article online at <https://doi.org/10.1016/j.celrep.2018.12.058>.

## ACKNOWLEDGMENTS

We thank James Macdonald and Saskia Brüers for help with data collection. This work was supported by an ERC Consolidator Grant–P-CYCLES (614244) awarded to R.V.

## AUTHOR CONTRIBUTIONS

R.V. designed and performed research. D.L.-S. analyzed data. D.L.-S. and R.V. wrote and reviewed the manuscript.

## DECLARATION OF INTERESTS

The authors declare no competing interests.

Received: August 27, 2018  
 Revised: November 4, 2018  
 Accepted: December 12, 2018  
 Published: January 8, 2019

## REFERENCES

- Alexander, D.M., Jurica, P., Trengove, C., Nikolaev, A.R., Gepshtein, S., Zvyagintsev, M., Mathiak, K., Schulze-Bonhage, A., Ruescher, J., Ball, T., and van Leeuwen, C. (2013). Traveling waves and trial averaging: the nature of single-trial and averaged brain responses in large-scale cortical signals. *Neuroimage* 73, 95–112.
- Arcaro, M.J., Honey, C.J., Mruczek, R.E.B., Kastner, S., and Hasson, U. (2015). Widespread correlation patterns of fMRI signal across visual cortex reflect eccentricity organization. *eLife* 4, e03952.
- Benjamini, Y., and Hochberg, Y. (1995). Controlling the false discovery rate: a practical and powerful approach to multiple testing. *J. R. Stat. Soc. Series B Stat. Methodol.* 57, 289–300.
- Berens, P. (2009). CircStat: a MATLAB toolbox for circular statistics. *J. Stat. Soft.* 37, 1–21.
- Brüers, S., and VanRullen, R. (2017). At what latency does the phase of brain oscillations influence perception? *eNeuro* 4, ENEURO.0078-17.2017.
- da Silva, F.H., van Lierop, T.H.M.T., Schrijer, C.F., and van Leeuwen, W.S. (1973). Organization of thalamic and cortical alpha rhythms: spectra and coherences. *Electroencephalogr. Clin. Neurophysiol.* 35, 627–639.
- Ermentrout, G.B., and Kleinfeld, D. (2001). Traveling electrical waves in cortex: insights from phase dynamics and speculation on a computational role. *Neuron* 29, 33–44.
- Fellinger, R., Gruber, W., Zauner, A., Freunberger, R., and Klimesch, W. (2012). Evoked traveling alpha waves predict visual-semantic categorization-speed. *Neuroimage* 59, 3379–3388.
- Halgren, M., Devinsky, O., Doyle, W.K., Bastuji, H., Rey, M., Mak-McCully, R., Chauvel, P., Ulbert, I., Fabo, D., Wittner, L., et al. (2017). The generation and propagation of the human alpha rhythm. *bioRxiv*. <https://doi.org/10.1101/202564>.
- Hillyard, S.A., Teder-Sälejärvi, W.A., and Münte, T.F. (1998). Temporal dynamics of early perceptual processing. *Curr. Opin. Neurobiol.* 8, 202–210.
- Hindriks, R., van Putten, M.J.A.M., and Deco, G. (2014). Intra-cortical propagation of EEG alpha oscillations. *Neuroimage* 103, 444–453.
- Hughes, J.R. (1995). The phenomenon of travelling waves: a review. *Clin. Electroencephalogr.* 26, 1–6.
- İlhan, B., and VanRullen, R. (2012). No counterpart of visual perceptual echoes in the auditory system. *PLoS One* 7, e49287.
- Klimesch, W., Hanslmayr, S., Sauseng, P., Gruber, W.R., and Doppelmayr, M. (2007). P1 and traveling alpha waves: evidence for evoked oscillations. *J. Neurophysiol.* 97, 1311–1318.
- Lalor, E.C., Pearlmutter, B.A., Reilly, R.B., McDarby, G., and Foxe, J.J. (2006). The VESPA: a method for the rapid estimation of a visual evoked potential. *Neuroimage* 32, 1549–1561.
- Lütkenhöner, B. (2003). Magnetoencephalography and its Achilles' heel. *J. Physiol. Paris* 97, 641–658.
- Marmarelis, P., and Marmarelis, V. (1978). *Analysis of Physiological Systems: The White-Noise Approach* (Plenum Press).
- Michel, C.M., Murray, M.M., Lantz, G., Gonzalez, S., Spinelli, L., and Grave de Peralta, R. (2004). EEG source imaging. *Clin. Neurophysiol.* 115, 2195–2222.
- Muller, L., Reynaud, A., Chavane, F., and Destexhe, A. (2014). The stimulus-evoked population response in visual cortex of awake monkey is a propagating wave. *Nat. Commun.* 5, 3675.
- Muller, L., Piantoni, G., Koller, D., Cash, S.S., Halgren, E., and Sejnowski, T.J. (2016). Rotating waves during human sleep spindles organize global patterns of activity that repeat precisely through the night. *eLife* 5, e17267.
- Muller, L., Chavane, F., Reynolds, J., and Sejnowski, T.J. (2018). Cortical travelling waves: mechanisms and computational principles. *Nat. Rev. Neurosci.* 19, 255–268.
- Nolte, G., Ziehe, A., Nikulin, V.V., Schlögl, A., Krämer, N., Brismar, T., and Müller, K.-R. (2008). Robustly estimating the flow direction of information in complex physical systems. *Phys. Rev. Lett.* 100, 234101.
- Nunez, P.L., Wingeier, B.M., and Silberstein, R.B. (2001). Spatial-temporal structures of human alpha rhythms: theory, microcurrent sources, multiscale measurements, and global binding of local networks. *Hum. Brain Mapp.* 13, 125–164.
- Oostenveld, R., Praamstra, P., Stegeman, D.F., and van Oosterom, A. (2001). Overlap of attention and movement-related activity in lateralized event-related brain potentials. *Clin. Neurophysiol.* 112, 477–484.
- Pfurtscheller, G., and Lopes da Silva, F.H. (1999). Event-related EEG/MEG synchronization and desynchronization: basic principles. *Clin. Neurophysiol.* 110, 1842–1857.
- Pitts, W., and McCulloch, W.S. (1947). How we know universals; the perception of auditory and visual forms. *Bull. Math. Biophys.* 9, 127–147.
- Prechtl, J.C., Bullock, T.H., and Kleinfeld, D. (2000). Direct evidence for local oscillatory current sources and intracortical phase gradients in turtle visual cortex. *Proc. Natl. Acad. Sci. USA* 97, 877–882.
- Saalmann, Y.B., Pinsk, M.A., Wang, L., Li, X., and Kastner, S. (2012). The pulvinar regulates information transmission between cortical areas based on attention demands. *Science* 337, 753–756.
- Sato, T.K., Nauhaus, I., and Carandini, M. (2012). Traveling waves in visual cortex. *Neuron* 75, 218–229.
- Scherg, M. (1990). Fundamentals of dipole source potential analysis. In *Auditory Evoked Magnetic Fields and Electric Potentials*, G.L. Romani, ed. (Karger), pp. 40–69.
- Shevelev, I.A., Kamenkovich, V.M., Bark, E.D., Verkhutov, V.M., Sharaev, G.A., and Mikhailova, E.S. (2000). Visual illusions and travelling alpha waves produced by flicker at alpha frequency. *Int. J. Psychophysiol.* 39, 9–20.
- VanRullen, R., and Macdonald, J.S. (2012). Perceptual echoes at 10 Hz in the human brain. *Curr. Biol.* 22, 995–999.
- Zhang, H., Watrous, A.J., Patel, A., and Jacobs, J. (2018). Theta and alpha oscillations are traveling waves in the human neocortex. *Neuron* 98, 1269–1281.e4.

## STAR★METHODS

### KEY RESOURCES TABLE

REAGENT or RESOURCE	SOURCE	IDENTIFIER
Software and Algorithms		
MATLAB	<a href="https://www.mathworks.com/products/matlab.html">https://www.mathworks.com/products/matlab.html</a>	RRID:SCR_001622
FieldTrip	<a href="http://www.fieldtriptoolbox.org">http://www.fieldtriptoolbox.org</a>	RRID:SCR_004849
EEGLAB	<a href="https://sccn.ucsd.edu/eeglab/index.html">https://sccn.ucsd.edu/eeglab/index.html</a>	RRID:SCR_007292
Psychophysics Toolbox	<a href="http://psychtoolbox.org/">http://psychtoolbox.org/</a>	RRID:SCR_002881
Circular Statistics	<a href="https://github.com/circstat/circstat-matlab">https://github.com/circstat/circstat-matlab</a>	RRID:SCR_016651

### CONTACT FOR REAGENT AND RESOURCE SHARING

Further information and requests for resources may be directed to and will be fulfilled by the Lead Contact, Rufin VanRullen ([rufin.vanrullen@cns.fr](mailto:rufin.vanrullen@cns.fr)).

### EXPERIMENTAL MODEL AND SUBJECT DETAILS

The data we report here in our Experiment 1 ( $n = 28$ ) was constituted by 8 subjects from Figure 2C from [VanRullen and Macdonald \(2012\)](#) (2 female; mean age 30.087 range 26 – 35) and 20 participants from [\(Brüers and VanRullen, 2017; 10 female; mean age 28.04, range 23 – 39\)](#). The sample from Experiment 2 ( $n = 10$ ) came entirely from Figure 4B in [VanRullen and Macdonald \(2012\)](#) (2 female; mean age 30.02, range 26 – 35). In accordance with the Declaration of Helsinki, all participants gave written informed consent before starting the experiment. This study was carried out in accordance with the guidelines for research at the “Centre de Recherche Cerveau et Cognition.”

### METHOD DETAILS

#### Design, Procedure and Materials

##### Stimuli generation

The generation of visual stimuli was performed as follows. White-noise visual luminance sequences were displayed within a disc of  $3.5^\circ$  radius on a black background. In Experiment 1, a single disc was presented in the vertical meridian centered at  $7.5^\circ$  above the fovea in [\(VanRullen and Macdonald, 2012\)](#) sample and at  $7^\circ$  in [\(Brüers and VanRullen, 2017\)](#). In Experiment 2, two independent white-noise luminance sequences were simultaneously displayed in two discs located in the left and right visual hemifields centered at  $7.5^\circ$  eccentricity on the horizontal meridian. In both experiments, the power spectrum of each randomly generated luminance sequence was normalized to have equal power at all frequencies. Each trial (6.25 s long) was initialized with random values from 0 to 1 drawn from a uniform distribution. Subsequently, we performed a Fourier transform of the time series, divided each resulting complex coefficient by its amplitude, and then applied an inverse Fourier transform to return to the time domain. The resulting time series were scaled to range from black ( $0.1 \text{ cd/m}^2$ ) to white ( $59 \text{ cd/m}^2$ ).

##### Experimental design

A prototypical trial started with a white fixation dot presented at the center of the screen that remained throughout the experiment. Participants were told to keep fixation on the dot and covertly monitor the disc to detect a 1 s target appearing inside the disc on a random 25% of trials reporting it at the end of the trials ( $n = 8$ ), see [\(VanRullen and Macdonald, 2012\)](#). In a separate sample ( $n = 20$ ), a single frame lighter circle surrounded by a darker ring was presented 2 – 4 times per trial. Here, participants were instructed to press a button as soon as they detected the target.

##### EEG analysis

Both target-present and target-absent trials were included in the cross-correlation analysis. In Experiment 2, at the beginning of the block, written instructions indicated to the participant whether they should pay attention to the left disc, to the right disc, or to both (3 block types). An exploratory analysis did not yield significant phase differences between attention conditions, and we thus pooled the data across the 3 block types to gain statistical power. After artifact rejection, a total of  $307.82 \pm 89.23$  and  $463.90 \pm 85.98$  (mean  $\pm$  std) trials per participant in Experiments 1 and 2 respectively were collected. In Experiment 1, based on previous research [\(Shevelev et al., 2000; Klimesch et al., 2007\)](#), we quantified the potential presence of periodic traveling waves by computing pairwise phase differences between non-contiguous midline sensors (Oz–Pz, POz–CPz, Pz–Cz). In Experiment 2, for each electrode, phase differences were computed between perceptual echoes in response to left and right stimuli, and between electrodes for a given visual

stimulation condition. In both experiments, for each participant, electrode and stimulation condition, we band-pass filtered (8 – 12 Hz) the perceptual echoes using a 4<sup>th</sup> order Butterworth filter. Subsequently, instantaneous analytic phase was obtained by taking the angle of the Hilbert-transformed band-pass filtered signal.

The template traveling wave propagation was calculated by measuring all pairwise phase differences  $\psi_i$  between the reference sensor POz and the rest of the EEG sensors. We chose POz because it displayed a strong perceptual echo in all participants, which is critical to obtain meaningful phase-differences. The template was based on the complex mean of phase differences over the significant time-samples (see below). The idealized wave template  $W$  was generated by combining two independent dimensions: a signal  $S$  that represents the instantaneous oscillatory value of the perceptual echo and a transparency  $M$  that represents the time-averaged amplitude of the echo coded as a transparency mask (see Figure S1). The signal  $S$  was generated using 64 sine functions, each comprising the phase lag or lead  $\psi$  at sensor  $i$ :

$$S_i(t) = \sin(2\pi ft + \psi_i)$$

where  $f$  was set at 10 Hz. The transparency dimension  $M$  (time-independent) was defined by:

$$M_i = (1 - A_i) * m$$

where the vector  $m$  (constant with gray color value; see Figure S1) was inversely weighted by the amplitude of the corresponding perceptual echo peak amplitude ( $A_i$ , with values between [0 1]) for sensor  $i$ . This means that sensors with low echo amplitudes had high gray values (less transparent) and sensors with high echo amplitude had low gray values (more transparent). Combining  $S_i(t)$  and  $M_i$ , we obtained the template wave  $W_i(t)$  that represented the two dimensions: the wave propagation (i.e., phase lag or lead between sine waves across the scalp) and the contribution of each electrode to the wave (i.e., transparency level). These two dimensions are represented in the 2D color bar in Figures 1D, 3B, and S1.

### Dipole modeling

The wave templates were used to compute a source reconstruction of electroencephalogram (EEG) activity by ECD. A single equivalent dipole was fitted for each of 12 time points across a cycle of the wave template; we were interested to see how the 12 dipoles would change location and/or orientation across the cycle. Dipole fitting assumes that voltage activity measured at the scalp can be mathematically described using a small number of point-like ECDs (Scherg, 1990). First, standard electrode locations were co-registered to an anatomical MRI template. This MRI was used to build a realistic shaped volume conduction model by means of the boundary element method (Oostenveld et al., 2001) and discretized into a grid with a 1 cm resolution. To source model the template traveling wave propagation, single dipole fitting was performed using nonlinear search to find, for every time point, the optimal dipole such that its location and moment (i.e., dipole orientation) minimize the difference between the model and the measured topography in the least-squares sense (maximum iterations = 1000). More formally, let the signal be represented by the time series  $X(t) = [x_1, x_2, \dots, x_N]^T$  where  $N$  is the number of time points reflecting the time varying cross-correlation values of the template echo function:

$$X_r(t) = Gq(t)S^T(t) + \varepsilon(t)$$

where  $G$  is the lead field matrix (channels by grid points) that weights how a given source  $S$  located in a specific grid position projects to the scalp sensors, and  $\varepsilon$  is the error term. The lead field matrix  $G$  is determined from the volume conduction model. The single dipole represents a location in Cartesian coordinates  $q(t) = \{q_x, q_y, q_z\}$  with different magnitudes  $\|q(t)\|$  and moments  $\theta(t) = q(t)/\|q(t)\|$  as a function of time. The goal of dipole fitting is to find, in our case, a single dipole whose magnitude and moment generate a source that minimizes the squared error  $J_{LS}$  between our data  $X(t)$  and the model:

$$J_{LS}(q, \theta)(t) = \|X(t) - G\{q, \theta\}(t)S^T(t)\|^2$$

The optimal solution to minimize the least-squares error at time point  $t$  is:

$$S^T = G^+ X$$

where  $G\{q, \theta\}^+$  is the pseudoinverse of  $G\{q, \theta\}$ . This results in the following expression:

$$J_{LS}(q, \theta) = \|X - G\{q, \theta\}(G\{q, \theta\}^+ X)\|^2$$

Dipole modeling of traveling wave propagation was performed on the template  $W_i(t)$ . The electric current dipole is an idealized model that is defined by two charges with equal and opposite polarity. This implies that a given source located in a specific brain area (i.e., fixed dipole location  $q$ ), can project to the scalp either a positive or a negative voltage, only by rotating its moment by  $\pi$  radians. Due to the symmetry of our wave templates, the propagation of the negative trough of the template must therefore follow the same trajectory as its positive peak, but half a cycle later in time and with its dipole orientation inverted. To overcome this potential limitation, we also dipole-fitted the positive rectification of the wave template  $W_i(t)$  as in (Hindriks et al., 2014), and we limited our fitting to one half of the wave cycle. To estimate the validity of our assumptions, we simulated three types of traveling waves and we reconstructed their scalp projections. To achieve this, we constructed a traveling wave model by setting the position and moment

of a set of dipoles undergoing oscillatory activity fluctuations with systematic phase differences. We used the forward model  $G$  to estimate the potential field distribution  $W$  at the scalp level:

$$W_{model}(t) = \sum_k^Q G\{q_k, \theta_k\}(t) \cos(2\pi ft + \tau)^T$$

A global traveling wave was defined with dipoles ( $Q = 12$ ) having different equally distant positions from occipital to frontal cortex, fitting a parabola function between the following three voxels expressed in MNI Cartesian coordinates (voxel 1 = [2.5cm -9.4cm -0.3cm], voxel 2 = [2.5cm -2.8cm 6.8cm], voxel 3 = [2.5cm 2.5cm 5.3cm]; see [Figures 1C, 3B, and S2–S4](#)). Dipole moment was rotated linearly to cover  $\pi$  radians in 12 steps. The spanning was defined in spherical coordinates from  $\pi/3$  to  $4\pi/3$  elevation ( $\varphi$ ) while azimuth ( $\theta$ ) was locked to  $\pi/2$  and transformed back to Cartesian coordinates. The parameter  $\tau$  is what determines the specific phase-delay activation between dipole locations ( $\tau = 2\pi/Q$ ).

A Local periodic traveling wave was modeled with the same parameters as the Global traveling wave, but with the dipoles fixed to a single position, i.e.,  $q_k = q_1$  for all  $k$ . The position was fixed to  $q_1 = [2.5cm -7.1cm 4.4cm]$ . As for the global wave, the moment was rotated linearly to cover  $\pi$  radians in 12 steps from  $\pi/3$  to  $4\pi/3$ . The phase-delay activation between dipole locations was also  $\tau = 2\pi/Q$ . This simulation also produced a posterior-to-anterior traveling wave on the scalp, but the underlying dipole rotation emulated a voltage propagation across local sulci/gyri ([Hindriks et al., 2014](#)).

The 2-dipole phase-lagged traveling wave was generated sitting two dipoles in occipital and parietal cortices (occipital:  $q_1 = [2.5cm -8.8cm 1.5cm]$ ; parietal:  $q_2 = [2.5cm -5.6cm 5.5cm]$ ), with fixed moment (occipital:  $\varphi = 4\pi/3$ ,  $\theta = \pi/2$ ; parietal:  $\varphi = 0.57\pi$ ,  $\theta = \pi/2$ ). To simulate the activation lag between the dipoles, we set the parameter  $\tau = \pi/2$ .

All models produce periodic traveling waves that propagate from posterior to anterior sensors ([Shevelev et al., 2000](#); [Klimesch et al., 2007](#)), similar to the one observed in Experiment 1.

### Source modeling

We chose ECD modeling to tentatively reconstruct sources of the periodic traveling waves found on scalp EEG in the two experiments. Due to limitations of inverse modeling ([Lütkenhöner, 2003](#); [Michel et al., 2004](#)) and the *a priori* unknown ground truth of the spatial configuration of the sources underlying periodic traveling waves, we dipole-fitted both the original (unrectified) wave template and its positive-rectified version. We built simulated datasets to demonstrate the rationale behind this approach. Using a realistic biophysical forward modeling, we generated three types of periodic traveling waves: Global (12 anatomically separated dipoles simultaneously oscillating but with a systematic phase lag), Local (12 anatomically co-localized dipoles of different orientations, simultaneously oscillating but with a systematic phase lag) and the 2-dipole phase-lagged (with only 2 oscillating sources having a phase-lag of  $\pi/2$ ). All three situations could produce traveling waves qualitatively comparable to the ones observed experimentally ([Figures 1D and S2B](#)). Fitting single ECD for each time point to both the positive-rectified template and the unrectified template, we empirically showed that positive rectification provides a more accurate description when the ground truth is a Global periodic traveling wave, whereas dipole position and orientation can be recovered more accurately using the unrectified template when the ground truth is a Local or a 2-dipole phase-lagged periodic traveling wave ([Figures 1D and S2](#)). Given that we do not know the ground truth for our empirical data, we reported the two solutions.

In Experiment 1 (single disc above fovea), the tentative ECD source reconstruction based on the positive rectified template suggested that the underlying wave likely propagated over bilateral parieto-occipital regions (occipital superior lobe, cuneus, precuneus and parietal superior lobe; [Figure 1D](#); [Figure S3](#), upper row). The non-rectified wave template yielded a more spatially constrained solution centered on bilateral parietal lobe (precuneus; [Figure 1D](#); [Figure S3](#), lower row). Concerning Experiment 2 (two discs located in left and right visual hemifields), ECD analysis on the positive rectified wave template tentatively revealed that each of the two waves propagated within the contralateral hemisphere relative to the stimulation site, from occipital to parietal cortex (mid temporal lobe, mid and superior occipital lobe, cuneus and precuneus, inferior and superior parietal lobe until the post-central midline; [Figures 3B and S4](#)). As in Experiment 1, the source localization of the non-rectified wave template produced clustered dipoles in regions of parieto-occipital lobe (mid and superior occipital lobe, cuneus and precuneus, inferior and superior parietal lobe; [Figures 3B and S4](#)). In conclusion, both ECD solutions (based on rectified or non-rectified templates) agreed on the likely parieto-occipital origin of the periodic traveling waves; however, the exact spatial extent of these waves was considerably larger for rectified than non-rectified templates, and thus remains difficult to determine.

### QUANTIFICATION AND STATISTICAL ANALYSIS

To estimate the time samples in which perceptual echoes in response to one (Experiment 1) or two (Experiment 2) flickering sequences showed consistent phase relations across participants, we computed the phase-locking factor (PLV) across participants of the phase difference as follows:

$$PLV(f, t) = \frac{1}{N} \left| \sum_{k=1}^N e^{-i(\varphi_k^f(f, t) - \varphi_k^f(f, t))} \right|$$

where  $\varphi$  is the alpha analytic phase of each sensor in a pair (Oz–Pz, POz–CPz, Pz–Cz; Experiment 1) or stimulus condition ( $l$ , left;  $r$ , right; Experiment 2), and  $N$  the number of participants. The PLV was averaged over sensors and compared to a surrogate distribution in which (i) the trials were randomly assigned to one of the two stimulus conditions, (ii) the PLV across participants was subsequently re-computed and combined across electrodes, and (iii) this procedure was repeated 6000 times. This way we determined the PLV distribution under the null hypothesis (i.e., no systematic phase relation across subjects between left versus right stimuli). Statistical significance ( $p$  values) was obtained by comparing the original PLV with the surrogate distribution for each respective time point. The FDR method was used to correct for multiple comparisons to avoid type I errors (Benjamini and Hochberg, 1995).

The statistical significance of pairwise sensor phase differences were statistically evaluated using one-sample mean angle test at alpha value = 0.05 against zero and using the Rayleigh test (`circ_mtest.m` and `circ_rtest.m`, respectively; (Berens, 2009)). Phase differences were performed across participants ( $n = 28$ , Experiment 1;  $n = 10$ , Experiment 2).

#### DATA AND SOFTWARE AVAILABILITY

Data and code are available from the corresponding author upon request.